Supplementary Information for the article

The 2022 hydraulic stimulation at Utah FORGE: investigating fracturing mechanisms and testing forecasting approaches

Federica Lanza[1*], Antonio P. Rinaldi[1], Luigi Passarelli[2], Vanille A. Ritz[1], Victor Clasen Repollés[1], Ryan Schultz[1], Federico Ciardo[3], Laura Ermert[5], Luca Scarabello[10], Nicolas Schmid[1], Peidong Shi[11], Katinka Tuinstra[1], Arnaud Mignan[6], Ben Dyer[4], Dimitrios Karvounis[4], Peter Meier[4], Kristine Pankow[7], Jim Rutledge[8], Joseph Moore[9], and Stefan Wiemer[1]

[1] Swiss Seismological Service, ETH Zürich, Switzerland
[2] INGV Bologna, Italy
[3] Northwestern University, USA
[4] Geo-Energie Suisse, Switzerland
[5] Univ. Grenoble Alpes, Univ. Savoie Mont Blanc, CNRS, IRD, Univ. Gustave Eiffel, ISTerre, France
[6] Mignan Risk Analytics GmbH, Switzerland
[7] University of Utah Seismograph Stations, UT, USA
[8] Santa Fe Seismic, NM, USA
[9] Energy and Geoscience Institute, University of Utah, UT, USA
[10]Department of Earth and Planetary Sciences, ETH Zürich
[11] Cardiff University, UK
*Corresponding author: federica.lanza@sed.ethz.ch

Contents of this file:

Text S1: Expanded details on the Utah FORGE 2022 stimulation

The Utah FORGE 2022 stimulation of well 16A (78)-32 was conducted in three consecutive stages. The first stage accounted for 677 m³, injected into a ~ 61 m (200 ft) open hole section at the toe of the well on April 17, 2022, during 139 minutes of pumping time between 02:58 and 05:16 UTC (20:58 to 23:16 local time). It followed a step-increasing pattern succeeded by a faster step-decreasing shut-in, with a maximum pressure of 42.3 MPa (Figure S1a). The second stage consisted of the injection of 443 m³ in a 6.1 m (20 ft) long perforated interval between the measured depths of 3,219 m (10,560 ft) and 3,225 m (10,580 ft) (i.e. approximately 2,570 m true vertical depth) on April 19, 2022, during 184 minutes of pumping time between 12:30 and 15:42 UTC (07:30 to 10:42 local time). It followed a step-increasing pattern, succeeded by a faster step-decreasing shut-in, with a maximum pressure of 48.8 MPa. A sudden stop of the injection occurred shortly before 15:00 UTC, but injection resumed to its maximum rate by 15:05 UTC (Figure S1b). The third stage consisted of the injection with proppants of 480 m³ in a 6.1 m (20 ft) long perforated interval between the measured depths of 3,085 m (10,120 ft) and 3,091 m (10,140 ft) (i.e., approximately 2,510 m true vertical depth) on April 21, 2022, during 140 minutes of pumping time between 13:38 and 15:58 UTC (08:38 to 10:58 local time). It followed a step-increasing pattern, succeeded by a faster step-decreasing shut-in, with a maximum pressure of 49.8 MPa (Figure S1c)

Text S2: Detailed derivation of the PCA in case of 3D distribution of data points

The $\boldsymbol{x} = (x_i, y_i, z_i)$ earthquake hypocenters in the geographic coordinate system (*East, North, Vertical*) can be represented by *3* x *n* matrix $\boldsymbol{X}$ where *n* represents the number of earthquakes in the catalog. In the following, bold font indicates matrix and vector notation while italic font indicates scalar quantities.

The mean centered matrix of data can be defined as

$$\boldsymbol{B} = \boldsymbol{X} - \boldsymbol{\mu_X}$$

where $\boldsymbol{\mu_X} = (\boldsymbol{\mu_x}, \boldsymbol{\mu_y}, \boldsymbol{\mu_z})$ is a vector of the row-means along each coordinate axis (coordinate centroid) and the rows vectors of **B** are the mean centered coordinates $\boldsymbol{x}^* = (x_i^*, y_i^*, z_i^*)$. The covariance matrix of $\boldsymbol{X}$ is:

$$\boldsymbol{C} = \frac{\mathbf{1}}{\boldsymbol{n-1}}\,\boldsymbol{B^T B}$$

We compute the eigenvector decomposition of the covariance matrix as:

$$\boldsymbol{C} = \boldsymbol{V^T \Lambda\ V}$$

where $\boldsymbol{V}$ is a rotation matrix composed by the eigenvectors $\boldsymbol{v_k}$ $(k = 1,2,3)$, $\boldsymbol{\Lambda} = \mathrm{diag}(\boldsymbol{\lambda})$ is the diagonal matrix of eigenvalues which represents the variance of $\boldsymbol{B}$ along each eigenvector $\boldsymbol{v_i}$ (Quinn & Ehlmann, 2019) and $\boldsymbol{C\,V = V\Lambda}$ and the principal components are $\mathbf{T = B\,V}$.

Numerically, the implementation of PCA, can be obtained via a singular value decomposition of the mean centered matrix that can be expressed as:

$$\boldsymbol{B = \ US\,V^T}$$

where $\boldsymbol{U\,U^T = \ V\,V^T = I}$ identity matrix and $\mathbf{S} = \mathrm{diag}(\mathbf{s})$ is the diagonal matrix containing the singular values $\mathbf{s_k}$ $(k = 1,2,3)$ of the data matrix $\mathbf{B}$ in decreasing order. Therefore, substituting the singular value decomposition of $\boldsymbol{B = \ US\,V^T}$ into the definition of principal components $\mathbf{T = B\,V}$, it can be obtained that $\boldsymbol{T = B\,V = U\,S}$, and in other words $\boldsymbol{T}$ are directions $\boldsymbol{U}$ (eigenvectors matrix) and magnitudes $\boldsymbol{S}$ (eigenvalues matrix) of the axes of the fitted ellipsoid. It can be easily shown that the singular values and the eigenvalues are related as:

$$\boldsymbol{\Lambda} = \frac{\boldsymbol{S}^2}{n-1}$$

which allows to recover the eigenvalues $\boldsymbol{\lambda}$, and the proportion of variance associated to a single principal component is $\pi_i = \ \lambda_i / \sum_{i=1}^{3} \lambda_i$ (Jollife & Cadima, 2016; Quinn & Ehlmann, 2019).

Supplementary Tables and Figures

Table S1: Overview of the statistical analysis of all the events with assigned magnitudes including poorly located events. [extended catalogue]

	All events with assigned magnitudes			
	Number of events	**Mc (MAXC+0.2) (M_w)**	***b*-value**	**N ≥ Mc**
Stage 1	3346	-1.33	2.98 ± 0.09	996
Stage 2	5456	-1.42	1.13 ± 0.02	2088
Stage 3	13135	-1.4	1.11 ± 0.01	5445

Table S2: Model parameters for the forecasting models EM, PI-ML and HM1D, respectively.

EM	Magnitude of completeness (Mc [-])	-1.19/**Calibrated**
	Magnitude distribution discretization (dM [-])	0.25
	b-value (b [-])	**Calibrated**
	Activation parameters (a_{fb} [-])	**Calibrated**
	Decay factor (τ [days])	**Calibrated**
	Number of simulation (Nsim)	100
	Inversion mode	Maximum Likelihood Estimate (MLE)
PI-ML	Magnitude of completeness (Mc [-])	-1.19/**Calibrated**
	Magnitude distribution discretization (dM [-])	0.25
	b-value (b [-])	**Calibrated**
	Number of multi-LASSO (LASSO_m)	50
	Minimum number of samples for fit (LASSO_Nmin_fit)	5
	Number of simulation (Nsim)	100
	Time discretization hydraulics (Delta_tau [s])	30 s
	Flow models	Both point source and theis' models
	Max grid extend flow model (max_grid_ext [m])	2000 m
	Cross-section point source (xsection [m^2])	90 m^2
	Layer thickness Theis' model (layer_thick [m])	30
	Storage (S [Pa^{-1}])	**Calibrated in range (10^{-15} – 10^{-5} Pa^{-1})**
	Permeability (k [m^2])	**Calibrated in range (10^{-20} – 10^{-12} m^2)**
HM1D	Time discretization hydraulics (Delta_tau [s])	30 s
	Forecast spacing (forecast_dx [m])	20 m
	Maximum iteration for inversion (max_iter_DE)	100
	Number of simulation (Nsim)	100
	Seismicity model	CAPS
	Magnitude of completeness (Mc [-])	-1.19/**Calibrated**
	Magnitude distribution discretization (dM [-])	0.25
	b-value (b [-])	**Calibrated**
	Seismicity density factor	**Calibrated in range (3000 – 3500)**
	Mean of maximum principal stress ($\sigma1$ [MPa])	63.9 MPa
	Standard deviation on $\sigma1$ ($\sigma_{\sigma1}$ [MPa])	**Calibrated in range (0.5 – 7.5 MPa)**
	Mean of minimum principal stress ($\sigma3$ [MPa])	41.85 MPa
	Standard deviation on $\sigma3$ ($\sigma_{\sigma3}$ [MPa])	**Calibrated in range (0.5 – 5.5 MPa)**
	Hydrostatic pressure (p_{hydro} [MPa])	24.8
	Cohesion (C [MPa])	3
	Friction coefficient (μ [-])	**Calibrated in range (0.5 – 0.75)**
	Retriggering	Enabled
	Scaling CAPS distribution	0.05
	Stoage (S [Pa^{-1}])	**Calibrated in range ($10^{-8.3}$ – $10^{-8.2}$ Pa^{-1})**
	Zero-stress aperture (b_0 [m])	**Calibrated in range (10^{-5} – 10^{-2} m)**
	Residual aperture (b_{res} [m])	**Calibrated in range (10^{-5} – 10^{-2} m)**
	Fracture normal stiffness (K_n [Pa])	10^{12} Pa
	Shearing fracture aperture magnitude (b_s [m])	**Calibrated in range (10^{-9} – 10^{-4} m)**
	Maximum shearing fracture aperture ($b_{s\,max}$ [m])	**Calibrated in range (10^{-7} – 10^{-4} m)**
	Fracture spacing (s_f [m])	1
	Scaling factor for shearing fracture aperture (γ [-])	**Calibrated in range (10^{-13} – 10^{-8})**
	Fracture aperture effect dumping factor (w [-])	**0.6**
	Normal stress (σ_n [MPa])	50.65 MPa
	Threshold pressure (p_{thr} [MPa])	45.18 MPa
	Max grid extend flow model (max_grid_ext [m])	2000 m

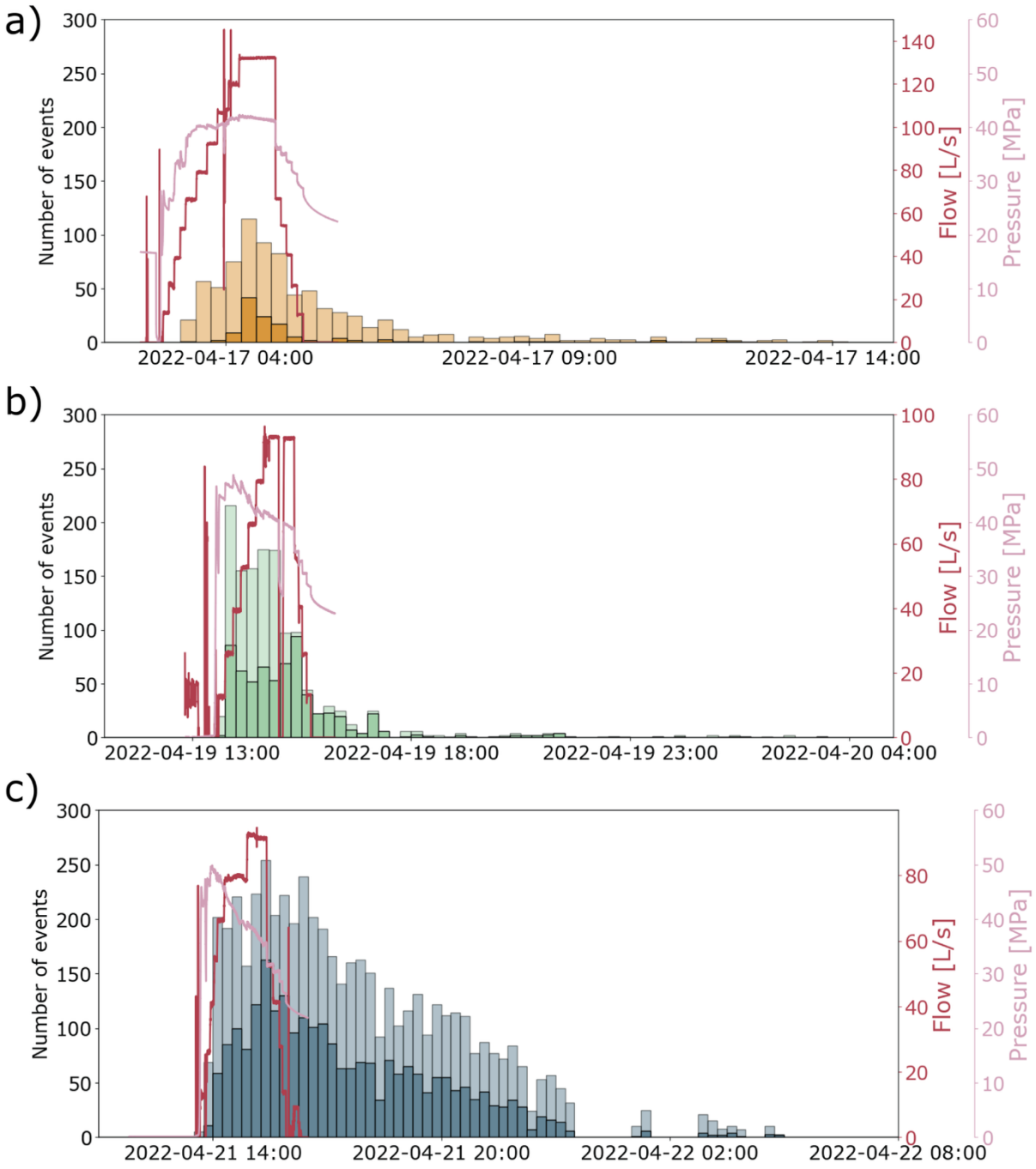

Figure S1: Histogram with number of earthquakes in total (light color) and above Mc (dark color) binned every 15 minutes along with flow rate and pressure for stage 1 (a), stage 2 (b) and stage 3 (c). [manually reviewed catalogue]

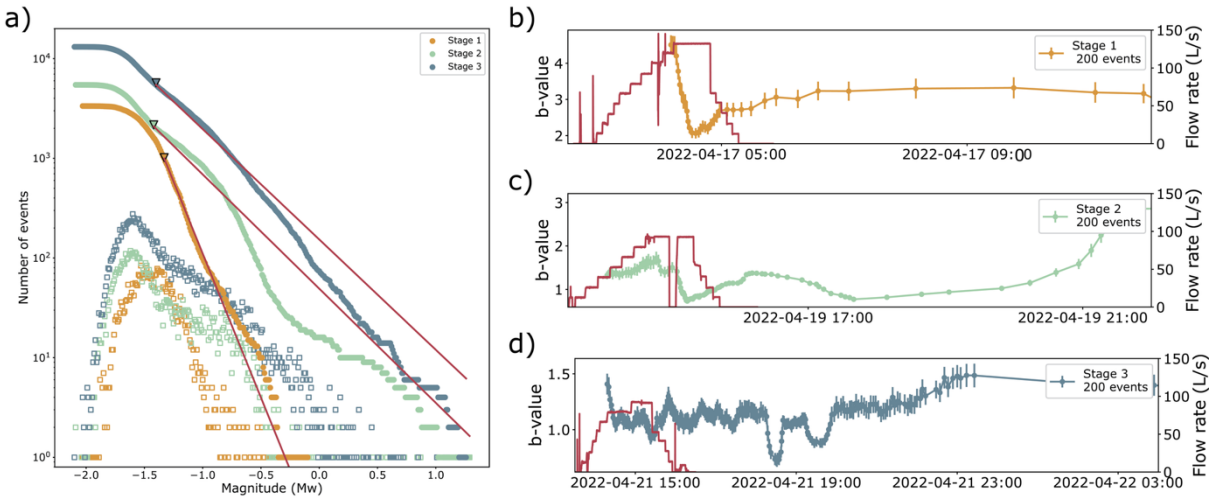

Figure S2: Statistical analysis of the full catalog (manual + automatic locations/magnitudes). a) Frequency-magnitude distribution. b, c, d) Temporal evolution of the *b*-value and injection rate for Stages 1, 2 and 3 (200 events window with completeness pre-filter).

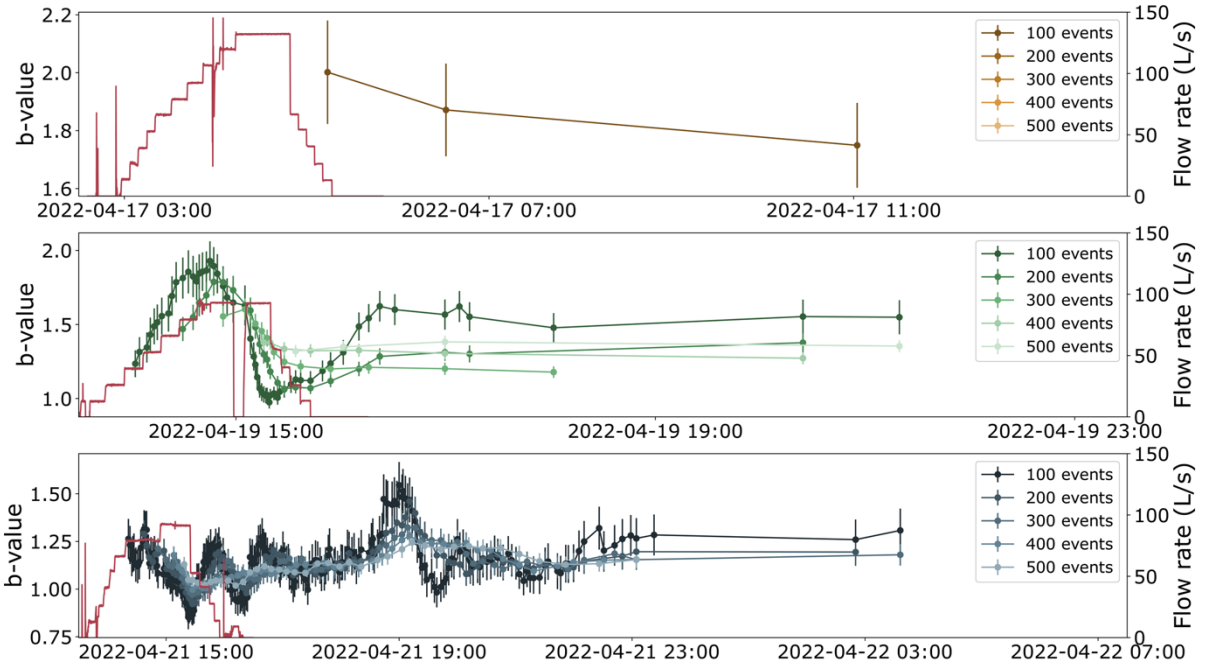

Figure S3: Evolution of the *b*-value in time for different events windows with 10% overlap (manually reviewed catalog, pre-filter with Mc). [manually reviewed catalogue]

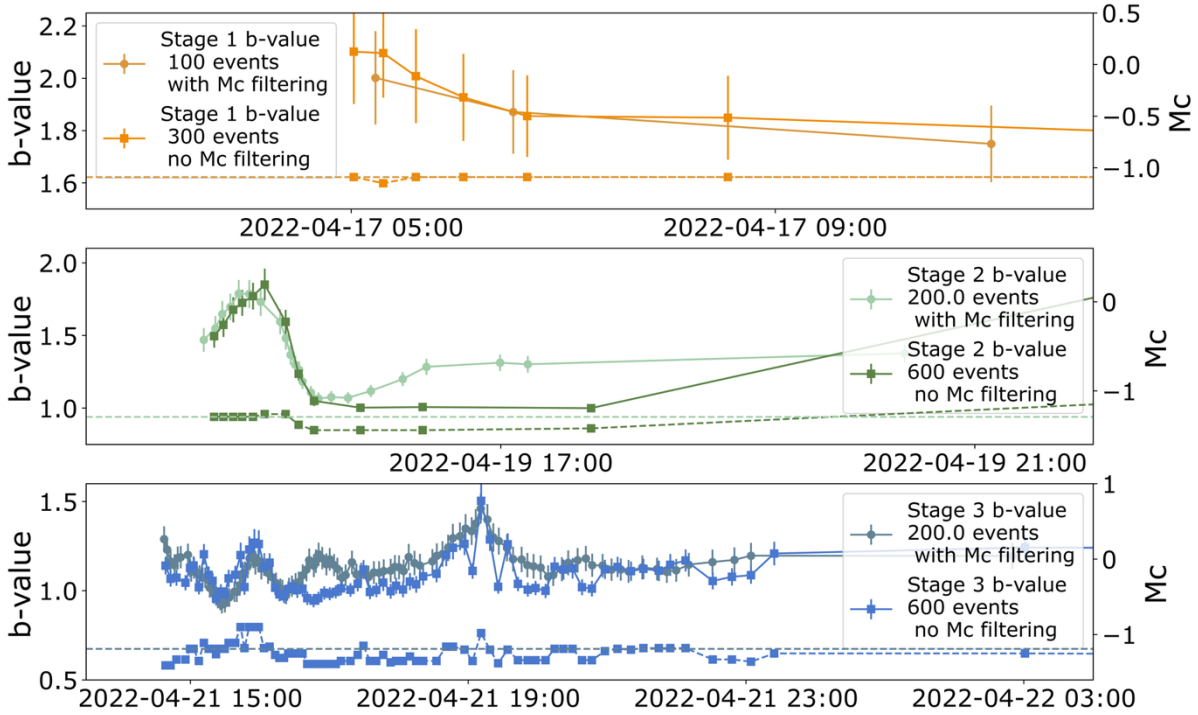

Figure S4: Comparison of the temporal evolution of the *b*-value with fixed Mc (pastel lines, as in the main text) and variable Mc calculated for each time bin (bright colours). The completeness used in each bin is indicated with the dashed lines. The number of events in the bins with variable Mc was adjusted to have a similar number of points in time as the results presented in the main text.

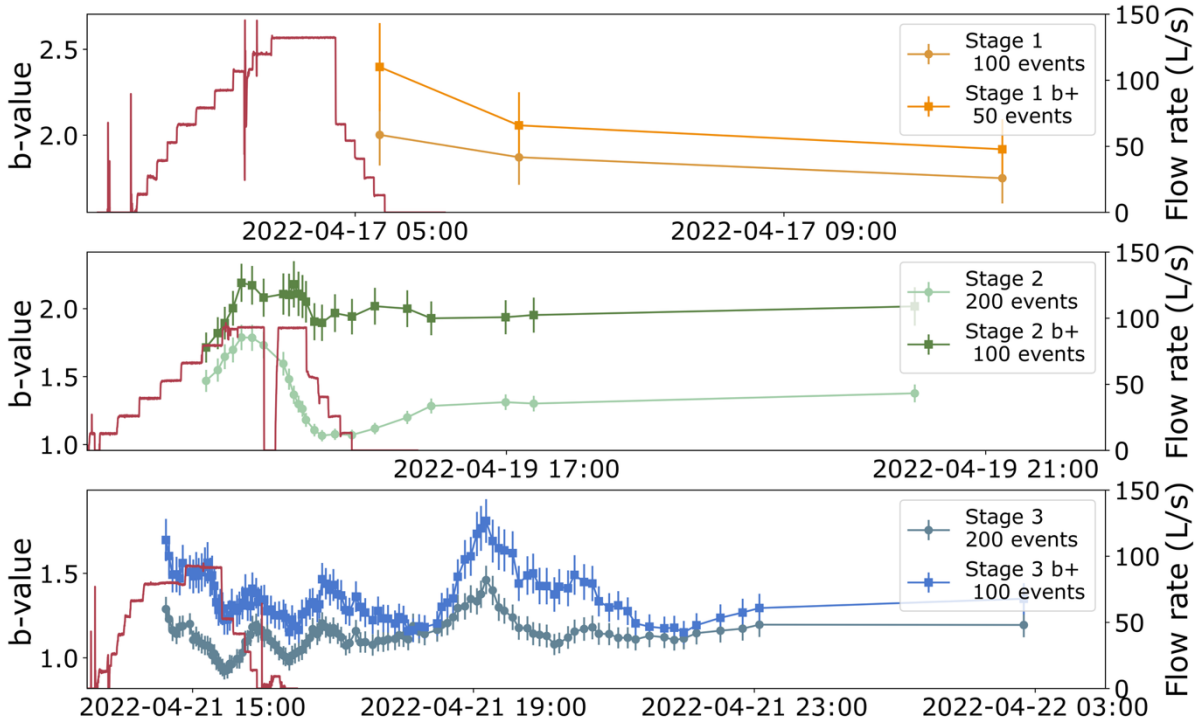

Figure S5: Comparison between the classical and *b*-positive approaches for *b*-value computation.

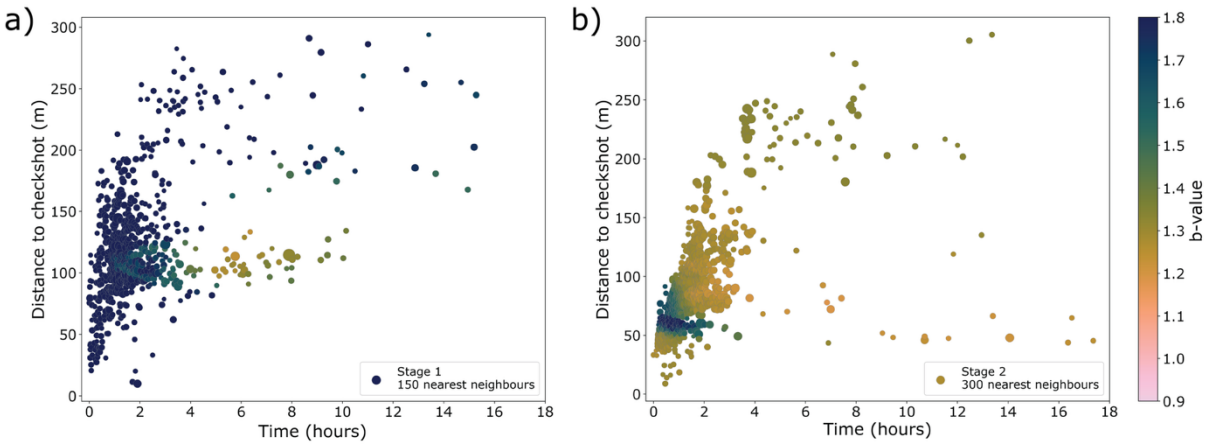

Figure S6: Time-distance plot for Stage 1 (left), Stage 2 (right), each event is colored by the *b*-value calculated using the 300 closest neighbors in a semi-normalized (distance-time) domain. The size of the dots indicates the magnitude of the event. [manually reviewed catalogue]

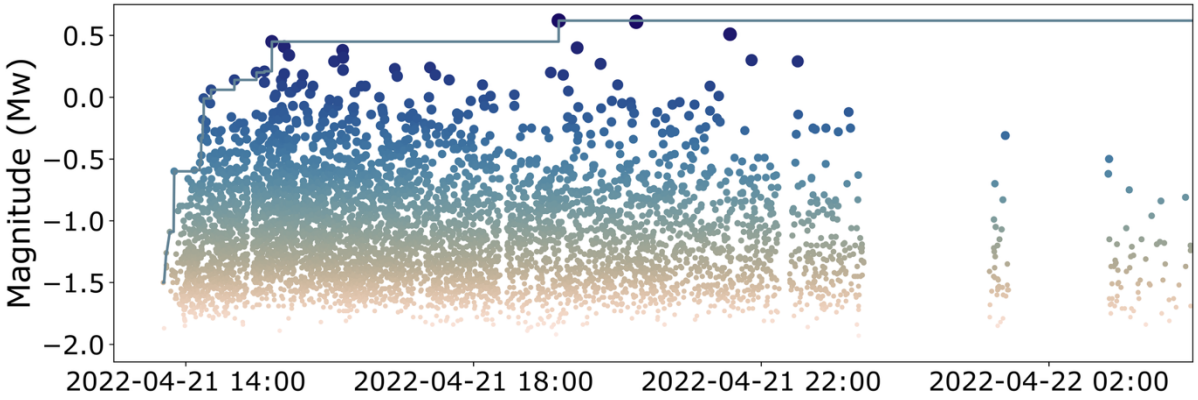

Figure S7: Timeline of the seismicity recorded during Stage 3 and evolution of the maximum observed magnitude (blue solid line).

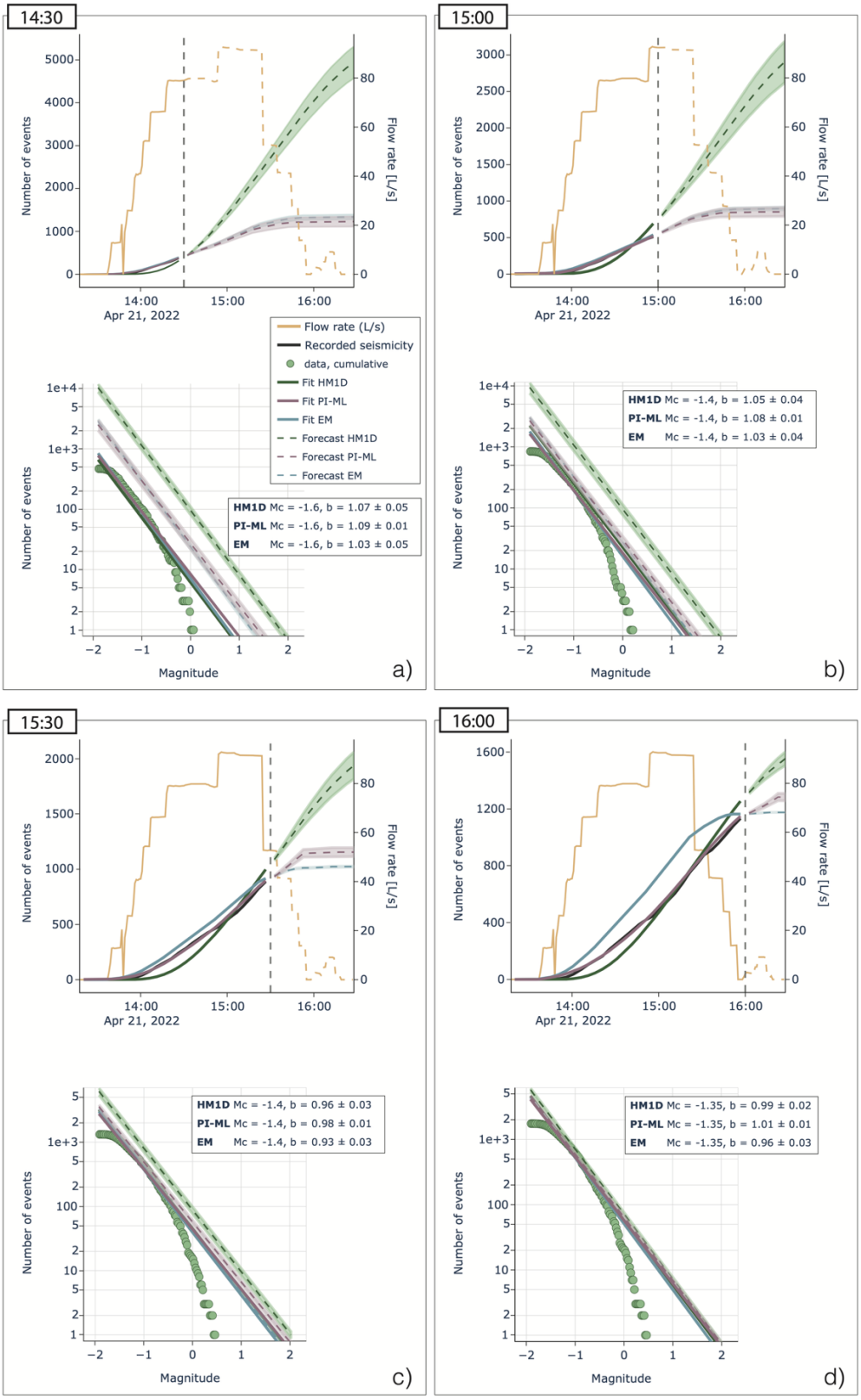

Figure S8: Four snapshots of the pseudo-forecast test with variable Mc at different t_{learn} (14:30, 15:00, 15:30, 16:00 UTC). Each panel shows on top the cumulative number of events simulated and recorded before t_{learn} (black dashed – line) as well as the forecast cumulative number of events with stochastic variability in the shaded area (green HM1D, purple PI-ML, blue EM). The bottom of each panel compares the recorded frequency-magnitude distribution with the fitted curve at t_{learn} as well as the forecasted distribution at the end of the stimulation.

Downloads available through the ETH Research Collection: https://doi.org/10.3929/ethz-c-000785663

Movie S1: Movie showing the spatial and temporal evolution of seismicity during Stage 3 of the April 2022 hydraulic stimulation at the Utah FORGE site. Symbol size scales with event magnitude. The injection point is marked by a black triangle, and the trajectory of well 16A-32 is shown as a thick black line. Regional principal stress orientations are indicated by arrows (after Xing et al., 2022).